CCR2 inhibition reduces tumor myeloid cells and unmasks a checkpoint inhibitor effect to slow progression of resistant murine gliomas

Joseph A. Flores-Toro[a], Defang Luo[a], Adithya Gopinath[a], Matthew R. Sarkisian[b], James J. Campbell[c], Israel F. Charo[c], Rajinder Singh[c], Thomas J. Schall[c], Meenal Datta[d], Rakesh K. Jain[d,1], Duane A. Mitchell[e,f], and Jeffrey K. Harrison[a,f,1]

[a]Department of Pharmacology & Therapeutics, College of Medicine, University of Florida, Gainesville, FL 32610; [b]Department of Neuroscience, College of Medicine, University of Florida, Gainesville, FL 32610; [c]ChemoCentryx, Mountain View, CA 94043; [d]Edwin L. Steele Laboratories, Department of Radiation Oncology, Massachusetts General Hospital, Harvard Medical School, Boston, MA 02114; [e]Department of Neurosurgery, College of Medicine, University of Florida, Gainesville, FL 32610; and [f]Preston A. Wells Jr. Center for Brain Tumor Therapy, University of Florida, Gainesville, FL 32610

Contributed by Rakesh K. Jain, November 27, 2019 (sent for review June 26, 2019; reviewed by Michael Lim and Michael Weller)

Immunotherapy directed at the PD-L1/PD-1 axis has produced treatment advances in various human cancers. Unfortunately, progress has not extended to glioblastoma (GBM), with phase III clinical trials assessing anti-PD-1 monotherapy failing to show efficacy in newly diagnosed and recurrent tumors. Myeloid-derived suppressor cells (MDSCs), a subset of immunosuppressive myeloid derived cells, are known to infiltrate the tumor microenvironment of GBM. Growing evidence suggests the CCL2–CCR2 axis is important for this process. This study evaluated the combination of PD-1 blockade and CCR2 inhibition in anti-PD-1–resistant gliomas. CCR2 deficiency unmasked an anti-PD-1 survival benefit in KR158 glioma-bearing mice. $CD11b^{+}/Ly6C^{hi}/PD\text{-}L1^{+}$ MDSCs within established gliomas decreased with a concomitant increase in overall $CCR2^{+}$ cells and MDSCs within bone marrow of CCR2-deficient mice. The CCR2 antagonist CCX872 increased median survival as a monotherapy in KR158 glioma-bearing animals and further increased median and overall survival when combined with anti-PD-1. Additionally, combination of CCX872 and anti-PD-1 prolonged median survival time in 005 GSC GBM-bearing mice. In both models, CCX872 decreased tumor associated MDSCs and increased these cells within the bone marrow. Examination of tumor-infiltrating lymphocytes revealed an elevated population, increased IFNγ expression, indicating enhanced cytolytic activity, as well as decreased expression of exhaustion markers in $CD4^{+}$ and $CD8^{+}$ T cells following combination treatment. These data establish that combining CCR2 and PD-1 blockade extends survival in clinically relevant murine glioma models and provides the basis on which to advance this combinatorial treatment toward early-phase human trials.

glioblastoma | immunotherapy | tumor microenvironment | myeloid-derived suppressor cells | programmed death-1

Glioblastoma (GBM), the most common malignant brain tumor in adults, presents a challenge for neurooncologists, as current therapies are minimally effective (1–8). Standard of care for GBM relies on initial surgical resection of the tumor mass followed by adjuvant radiation and chemotherapy with temozolomide. However, these approaches yield only moderate increase in survival rates, with current median survival for GBM reported at 14.9 mo, with a <10% 5-y survival rate (1, 9). Attempts to target the immune system have presented encouraging preclinical outcomes (10–12) as well as in some early-phase trials (13, 14) but have failed to show progress in randomized phase III clinical trials for either recurrent (CheckMate 143; ClinicalTrials.gov Identifier NCT02017717) or newly diagnosed GBM (CheckMate 498; ClinicalTrials.gov Identifier NCT02617589) (15). Overcoming the highly immune-suppressive environment characteristic of GBM is paramount. Approaches utilizing inhibitors of immune-suppressive mechanisms that directly promote tumor progression and/or contribute to the immune-suppressed environment are under investigation. In all likelihood, an immune-based approach for GBM will require the use of a combination of therapies to achieve durable remissions.

GBMs can impact immune responses via multiple mechanisms that include manipulation of distant tissues, e.g., promoting sequestration of T cells within the bone marrow (16). Antitumor T cell responses are also regulated by costimulatory and coinhibitory signals that comprise the immune-checkpoint system. Recent advances in immune-based therapies have targeted this system via development of monoclonal antibodies directed

Significance

Standard of care for glioblastoma (GBM) results in median survival of <15 mo with 5-y survival <10%, highlighting the need for novel treatments. Immune checkpoint blockade has been successful in various cancer subtypes. However, success has not extended to GBM, largely due to the characteristically immune-suppressive glioma microenvironment. Here, we report targeting of myeloid derived suppressor cells (MDSCs), via inhibition of CCR2, unmasks efficacy of checkpoint blockade in GBM. Using checkpoint inhibitor-resistant murine glioma models, we show combination treatment reduces MDSCs and increases functional T cells within the tumors, and significantly extends overall survival. Our results support targeting of CCR2-expressing myeloid cells to enhance immunotherapies for GBM, and warrant translation of this approach to early human clinical trials.

Author contributions: J.A.F.-T., J.J.C., R.S., R.K.J., D.A.M., and J.K.H. designed research; J.A.F.-T., D.L., A.G., M.R.S., and M.D. performed research; J.J.C., I.F.C., R.S., and T.J.S. contributed new reagents/analytic tools; J.A.F.-T., D.L., A.G., M.R.S., and M.D. analyzed data; and J.A.F.-T., M.D., R.K.J., D.A.M., and J.K.H. wrote the paper.

Reviewers: M.L., The Sidney Kimmel Comprehensive Cancer Center at Johns Hopkins Hospital; and M.W., University Hospital of Zurich.

Competing interest statement: J.J.C., I.F.C., R.S., and T.J.S. are all employed by ChemoCentryx and are stockholders. D.A.M. holds patented technologies that have been licensed or have exclusive options to license to Celldex Therapeutics, Annias, Immunomic Therapeutics, and iOncologi. D.A.M. receives research funding from Immunomic Therapeutics. D.A.M. serves as an advisor/consultant to Bristol-Myers Squibb, Tocagen, and Oncorus. D.A.M. is cofounder of iOncologi, Inc., an immunooncology biotechnology company. Neither any reagent nor any funding from these organizations was used in this study. J.A.F.-T., D.L., A.G., M.R.S., M.D., and J.K.H. have no competing interests to report. R.K.J. received honorarium from Amgen; consultant fees from Chugai, Merck, Ophthotech, Pfizer, SPARC, SynDevRx, XTuit; owns equity in Enlight, Ophthotech, SynDevRx; and serves on the Boards of Trustees of Tekla Healthcare Investors, Tekla Life Sciences Investors, the Tekla Healthcare Opportunities Fund, and the Tekla World Healthcare Fund. Neither any reagent nor any funding from these organizations was used in this study.

[1]To whom correspondence may be addressed. Email: jain@steele.mgh.harvard.edu or jharriso@ufl.edu.

This article contains supporting information online at https://www.pnas.org/lookup/suppl/doi:10.1073/pnas.1910856117/-/DCSupplemental.

First published December 26, 2019.

against either programmed death-1 or its ligand, i.e., PD-1/PD-L1. Tumor cells exploit the PD-1/PD-L1 axis as a means to evade immune surveillance by expressing PD-L1. The receptor for PD-L1, PD-1, is expressed by T cells and, when stimulated, acts to inhibit T cell activation/effector function. The use of checkpoint inhibitors in certain cancers such as melanoma (17, 18), lung (19), renal cell carcinoma (20), colon (21), and hepatocellular carcinoma (22, 23) has proven effective. Although intratumoral expression of PD-L1 in GBM has been observed, correlations with patient outcome have been inconclusive or inconsistent (24–26). Despite discrepancy in the prognostic ability of PD-L1 expression, these studies posit that the use of immune-checkpoint inhibitor-based approaches is warranted, although this line of therapy has failed as a single treatment in recurrent and newly diagnosed GBM. While the reasons for these incomplete response rates are poorly understood, it has been shown that a small subset of GBM patients presenting with higher than typical mutational load respond well to anti-PD-1 therapy (27). The success of PD-1 blockade in these patients suggests checkpoint blockade may be a viable therapy for GBM. Moreover, the recent demonstration that neoadjuvant PD-1 blockade provided a benefit for GBM patients over adjuvant therapy has renewed interest in immune-checkpoint inhibitor therapy in GBM (13, 14). Preclinical studies aimed at augmenting the efficacy of checkpoint blockade via combinatorial approaches targeting the immune suppressive microenvironment are ongoing (28–32).

A subset of myeloid-derived cells with immunosuppressive properties, termed myeloid-derived suppressor cells (MDSCs), are known to be elevated in the peripheral blood of GBM patients (33). MDSCs infiltrate the glioma microenvironment, and act as drivers of the immune-suppressive phenotype typical of these tumors (33–42). The mechanism by which they traffic to the tumor site is not entirely clear, although growing data suggest chemokine receptors are important for this process, namely chemokine receptor 2 (CCR2) (40, 43–48). Indeed, previous reports indicate Ly6C^{hi} inflammatory monocytes express CCR2 (43). Additionally, known ligands of this receptor (CCL2 and CCL7) are expressed by gliomas and are thought to mediate tumor recruitment of CCR2^{+} cells (40, 44, 47, 49, 50). Approaches that specifically target the MDSC population have been employed in various tumor types where they have been shown to enhance immunogenicity and, in some cases, even reverse resistance to checkpoint blockade (51–55).

In this study, we sought to more clearly define the role of CCR2 in immune-checkpoint inhibitor-resistant high-grade gliomas. Using CCR2-deficient mice, we report loss of CCR2 expression prevented egress of MDSCs from the bone marrow, reduced glioma infiltration of these cells, and unmasked an anti-tumor effect of PD-1 blockade. Further, use of a CCR2 antagonist, CCX872, recapitulated the findings of genetic ablation, demonstrating reductions in MDSC glioma infiltration and imparting an enhanced anti-PD-1 survival effect. Taken together, we suggest that disruption of the CCL2/CCR2 axis promotes sequestration of CCR2^{+} cells within bone marrow, limiting distribution of these immune-suppressive cells to the tumor, and allowing for attenuation of the immunosuppressive tumor microenvironment. As such, the amelioration of immune suppression via CCR2 inhibition may contribute to enhanced anti-PD-1 efficacy in gliomas.

Results

Distinct CCR2- and CX3CR1-Expresssing Myeloid Cell Populations in Glioma-Bearing Mice. CCR2^{+} cells do not represent the sole myeloid cell type present in gliomas, as CX3CR1^{+} central nervous system (CNS)-resident microglia are known to infiltrate as well. As a means to investigate the glioma presence of these chemokine receptor-expressing myeloid cell populations, we employed double transgenic mice that carry RFP in place of the CCR2 gene (CCR2$^{RFP/WT}$) and GFP in place of CX3CR1 (CX3CR1$^{GFP/WT}$) as knock-in alleles, enabling direct surveillance of CCR2^{+} and CX3CR1^{+} cells. Two therapy-resistant murine glioma models were employed, including the high-grade glioma KR158 model and the recently reported GBM stem-like cell 005 GSC model (56–58). These models exhibit common histological characteristics of glioma, including areas of increased cell density, necrotic regions within the tumor, invasion of normal brain parenchyma, and pseudopalisading necrosis (*SI Appendix*, Fig. S1 *A–C*), consistent with previously published results (56).

Fluorescent imaging confirmed the presence of both CCR2^{+} and CX3CR1^{+} cells within KR158 tumors (Fig. 1*A*). Flow-cytometric analysis identified tumor-associated CCR2^{+} and CX3CR1^{+} cells in both glioma models. However, the presence of both populations was significantly higher in KR158 tumors (CCR2^{+}, $P = 0.048$; CX3CR1^{+}, $P = 0.012$) (Fig. 1*B*). Analysis of the bone marrow revealed a significant increase in CCR2^{+} cells upon either KR158 ($P = 0.032$) or 005 GSC ($P = 0.001$) tumor implantation, with no change in this cell population as a result of phosphate-buffered saline (PBS) injection (Fig. 1*C*). The GFP^{+}/RFP^{+} cell population (CCR2^{+}/CX3CR1^{+}) was unchanged in the bone marrow of the tumor-bearing animals.

We next sought to characterize the myeloid marker phenotypes of the CCR2^{+} and CX3CR1^{+} populations in the tumor microenvironment. In order to investigate these populations, tumor infiltrates from glioma-bearing CCR2$^{RFP/WT}$;CX3CR1$^{GFP/WT}$ mice were subjected to flow-cytometric analysis of CD45, CD11b, Ly6C, and Ly6G. Two distinct CD45^{+} populations were identified, designated CD45^{low} and CD45^{hi} (Fig. 1*D*). Analysis of these populations revealed CD45^{low} events (Fig. 1 *D*, *Upper*) represent a cell population that is primarily CX3CR1^{+}, likely representing microglia. CD45^{hi} (Fig. 1 *D*, *Middle*) events represent a more heterogeneous cell population consisting of CCR2^{+}, CX3CR1^{+}, and CCR2^{-}/CX3CR1^{-} cells. Murine monocytic MDSCs are typically classified as CD11b^{+}/Ly6C^{hi}/Ly6G^{-}. To examine the heterogeneous CD45^{hi} population, we scrutinized CCR2^{+} and CX3CR1^{+} populations by expression of CD11b/Ly6C/Ly6G. Flow-cytometric analysis of Ly6C/Ly6G noted 3 distinct Ly6C populations: negative, intermediate, and high (Fig. 1*E*). Ly6G expression was minimal in the tumors. Ly6C^{hi} events (Fig. 1 *E*, *Upper*) represented a cell population that is primarily CCR2^{+}/CX3CR1^{+}, while Ly6C^{-} (Fig. 1 *E*, *Lower*) events consist of CCR2^{+}, CX3CR1^{+}, and CCR2^{-}/CX3CR1^{-} cells. Ly6C^{inter} events were determined to be CCR2/CX3CR1 double-positive (*SI Appendix*, Fig. S2*B*). Similar analysis within bone marrow isolates revealed 4 distinct populations: negative, Ly6C^{inter}/Ly6G^{-}, Ly6C^{hi}/Ly6G^{-}, and Ly6C^{inter}/Ly6G^{+} (*SI Appendix*, Fig. S2*C*). Ly6C^{hi}/Ly6G^{-} events were primarily CCR2^{+}/CX3CR1^{+}, while Ly6C^{-}/Ly6G^{-}, Ly6C^{inter}/Ly6G^{-}, and Ly6C^{inter}/Ly6G^{+} events were predominantly CCR2^{-}/CX3CR1^{-}. Tumor associated Ly6C^{hi} cells were PD-L1^{+}, although other cell populations express PD-L1 as well (*SI Appendix*, Fig. S2*D*).

Additional flow-cytometric analysis of CCR2- and CX3CR1-expressing cells determined that CCR2^{+}/CX3CR1^{-} cells were MHCII^{+}/F4/80^{-}/CD11c^{+}/CD11b^{lo}, CCR2^{+}/CX3CR1^{+} cells were MHCII^{+}/F4/80^{+}/CD11c^{+}/CD11b^{hi}, and CCR2^{-}/CX3CR1^{+} cells were MHCII^{+}/F4/80^{+}/CD11c^{-}/CD11b^{medium} (*SI Appendix*, Fig. S3 *A–D*). Taken together, invading myeloid cells expressing the 2 chemokine receptors within the tumor microenvironment are predominantly CCR2^{+} or CCR2^{+}/CX3CR1^{+} double-positive, while resident myeloid-like cells are predominantly CX3CR1^{+}.

CCR2 Deficiency Unmasks an Anti-PD-1 Effect in Immune-Checkpoint Inhibitor-Resistant Glioma. To establish a role of CCR2 in glioma and the potential impact of disrupting this receptor on the efficacy of immune-checkpoint inhibitors, we evaluated the effect of anti-PD-1 monotherapy in CCR2-sufficient and -deficient mice. In KR158 tumor-bearing (n = 8 to 10/group) CCR2$^{RFP/WT}$ or CCR2$^{RFP/RFP}$ mice, we dosed with anti-PD-1 starting at day 7, as

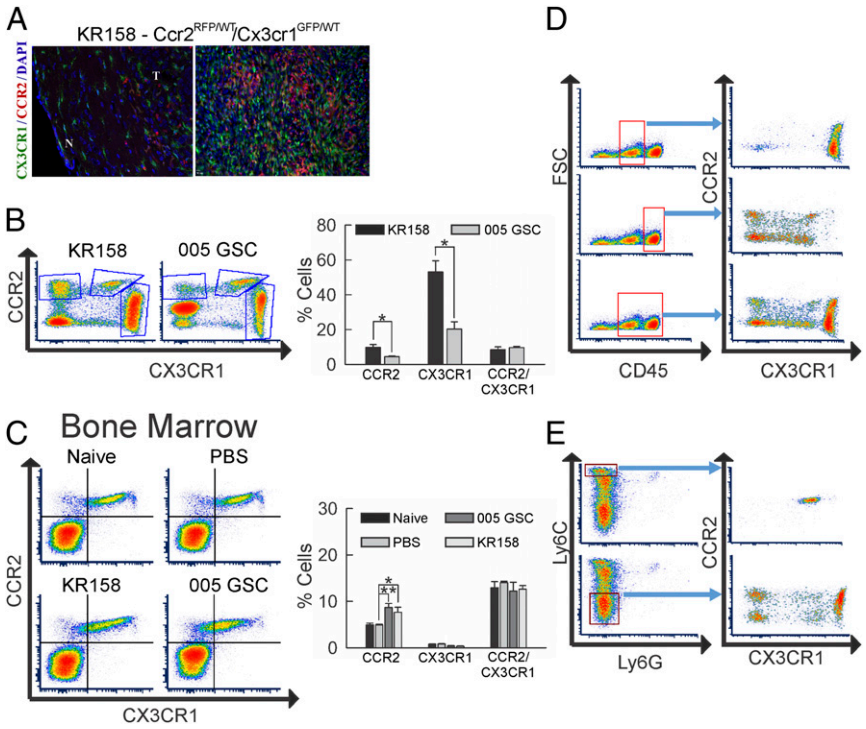

Fig. 1. Distinct cell populations of CCR2- and CX3CR1-expressing myeloid cells in glioma-bearing mice. (*A*) Fluorescent images showing representative example of section of KR158 tumor-bearing $Ccr2^{RFP/WT}/Cx3cr1^{GFP/WT}$ normal (N) and tumor (T) tissue. Red fluorescence denotes $CCR2^+$ cells, while green fluorescence denotes $CX3CR1^+$ cells. (Image magnification: 20×.) (*B*) Flow-cytometric analysis of tumor isolates from KR158 ($n = 4$) (*Left*) and 005 GSC ($n = 3$) (*Right*) tumor-bearing $Ccr2^{RFP/WT}$;$Cx3cr1^{GFP/WT}$ mice. Higher CCR2 single-positive ($P = 0.048$) and CX3CR1 single-positive ($P = 0.012$) cell populations in KR158 vs. 005 GSC glioma models are noted. (*C*) Flow-cytometric analysis of bone marrow cell populations in CCR2/RFP vs. CX3CR1/GFP in naïve ($n = 3$) (*Upper Left*), mock PBS-injected ($n = 6$) (*Upper Right*), 005 GSC ($n = 3$) (*Lower Left*), and KR158 ($n = 6$) (*Lower Right*) tumor-bearing $Ccr2^{RFP/WT}$;$Cx3cr1^{GFP/WT}$ animals. Quantification shows increase in CCR2 single-positive cells in KR158 ($P = 0.032$) and 005 GSC ($P = 0.001$) tumor-bearing animals. (*D*) Flow-cytometric analysis of tumor isolates from $Ccr2^{RFP/WT}$;$Cx3cr1^{GFP/WT}$ mice. The left graphs represent forward scatter (FSC) vs. CD45 plots demonstrating 3 CD45 populations: negative (left), low (middle), and high (right). Blue arrows denote subpopulations plotted by expression of CCR2 and CX3CR1. $CD45^{low}$ events (*Upper*) represent a primarily $CX3CR1^+$ cell population, while $CD45^{hi}$ events represent a heterogeneous cell population consisting of $CCR2^+$, $CX3CR1^+$, and $CCR2^-$/$CX3CR1^-$ cells. (*E*) Flow-cytometric analysis of tumor isolates from $Ccr2^{RFP/WT}$;$Cx3cr1^{GFP/WT}$ mice. The left graphs represent $Ly6C^+$ vs. $Ly6G^+$ events and demonstrate 3 Ly6C populations: negative (bottom), intermediate (middle), and high (top). Blue arrows denote subpopulations plotted by expression of CCR2 and CX3CR1. $Ly6C^{hi}$ events represent a cell population that is primarily $CCR2^+$/$CX3CR1^+$, while $Ly6C^-$ events represent a heterogeneous cell population consisting of $CCR2^+$, $CX3CR1^+$, and $CCR2^-$/$CX3CR1^-$ cells. Representative plots are shown throughout. $^*P < 0.05$; $^{**}P < 0.01$.

described in *Materials and Methods* and followed until humane end point (Fig. 2*A*). Survival analysis indicated no change in either median or durable survival due to CCR2 deficiency alone or anti-PD-1 monotherapy as compared to CCR2-sufficient/non–immune-checkpoint inhibitor-treated mice. However, when anti-PD-1 was administered to CCR2-deficient mice, a significant increase ($P = 0.035$) in overall durable survival was observed; differences in median survival between anti-PD-1 monotherapy-treated strains (24 vs. 35 d) did not reach statistical significance. For proof of concept in high mutational-burden tumors, we found CCR2 deficiency also augmented PD-1 blockade in GL261 tumor-bearing animals, with differential outcomes based on initial treatment time and total dosing of the antibody (*SI Appendix*, Fig. S4). Indeed, the variation in responses of GL261 gliomas to anti-PD-1 monotherapy is known (30).

CCR2 Deficiency Has Reciprocal Effects on Presence of MDSCs in Tumor and Bone Marrow. Imaging analysis of CCR2 promoter-driven RFP and staining for the myeloid marker CD11b confirmed the presence of $CCR2^+$ myeloid derived cells within KR158 gliomas (Fig. 2*B*). The presence of these cells was reduced in KR158 tumors from CCR2-deficient mice. Fluorescence imaging of bone marrow revealed significantly elevated CCR2/RFP signal (reported as pixel density vs. area of the cross-section) in non–tumor-bearing CCR2-deficient mice ($P = 0.029$) as compared to CCR2-sufficient animals. Further elevation was observed in both $CCR2^{RFP/WT}$ ($P = 0.011$) and $CCR2^{RFP/RFP}$ ($P = 0.036$) following KR158 tumor implantation (Fig. 2*C*).

Flow-cytometric analysis of the tumor-associated RFP^+ cell population revealed a statistically significant decrease ($P = 0.047$) of this population, while similar analysis of bone marrow showed a significant increase ($P = 0.024$) (Fig. 3*A*) in CCR2-deficient tumor-bearing mice. Not all $CCR2^+$ cells were found to be $Ly6C^+$. In order to more accurately examine the effect of CCR2 deficiency on the immune-suppressive cell population of these mice, flow-cytometric analysis of immune cells isolated from tumors and bone marrow of $CCR2^{RFP/WT}$ and $CCR2^{RFP/RFP}$ mice was performed. Analysis revealed a statistically significant reduction ($P = 0.039$) of MDSCs ($CD45^{hi}$/$CD11b^+$/$Ly6C^{hi}$) within KR158 tumors with a concomitant increase ($P = 0.020$) in bone marrow (Fig. 3*B*). Additionally, investigation of this population in the periphery was performed, and a significant reduction ($P = 0.048$) in the MDSC population present within spleens of tumor-bearing animals was evident (*SI Appendix*, Fig. S5*A*). The proportion of RFP^+ cells that are also $Ly6C^{hi}$ within the bone marrow is unchanged by CCR2 deficiency (Fig. 3*C*). However, when this proportion was determined in tumors, a marked reduction ($P = 0.007$) of this population was noted with CCR2 deficiency.

It has been reported that MDSCs residing within the tumor microenvironment prevent the entry of $CD8^+$ T cells into the

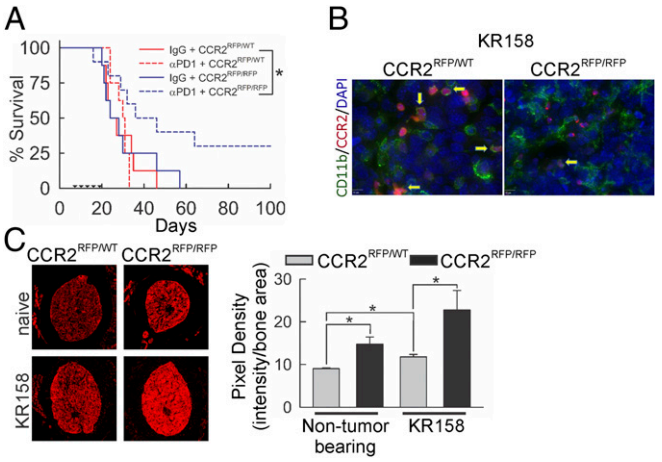

Fig. 2. Effect of Ccr2 deficiency on glioma-bearing mice. (*A*) Survival analysis of KR158 tumor-bearing $Ccr2^{RFP/WT}$ and $Ccr2^{RFP/RFP}$ mice treated with or without anti-PD-1. Ccr2 deficiency did not impact survival in IgG-treated $Ccr2^{RFP/WT}$ mice ($n = 8$), while anti-PD-1 treatment ($n = 10$) enhanced survival ($P = 0.035$) in Ccr2-deficient mice only. Triangles mark anti-PD-1 administration. (*B*) Fluorescent imaging of CD11b (green stain) in $Ccr2^{RFP/WT}$ and $Ccr2^{RFP/RFP}$ mice. Representative images shown. (*C*) Fluorescent imaging of femur cross-section from $Ccr2^{RFP/WT}$ and $Ccr2^{RFP/RFP}$ naive and KR158 tumor-bearing mice. Loss of Ccr2 enhanced CCR2/RFP signal in bone marrow of naive mice ($P = 0.029$), which was further enhanced in tumor-bearing $Ccr2^{RFP/RFP}$ animals ($P = 0.036$). Representative images are shown. Quantification: average pixel density/cross-sectional area from 3 consecutive sections, 3 mice/treatment group. $*P < 0.05$.

tumor (59). Despite a noted reduction in MDSCs within tumors, an increase in $CD4^+$ T cells ($P = 0.031$) was observed, while the population of $CD8^+$ T cells remained unaltered by CCR2 knockout (*SI Appendix*, Fig. S5*B*). A significant increase ($P = 0.003$) of the ratio of $CD8^+$ T cells/MDSCs was evident within tumors derived from CCR2-deficient mice (*SI Appendix*, Fig. S5*C*).

CCR2 Antagonist CCX872 Enhances an Anti-PD-1 Effect to Improve Survival. Given the enhanced anti-PD-1 effect in CCR2-deficient KR158 tumor-bearing mice, we hypothesized that pharmacological antagonism of CCR2 would augment the efficacy of immune-checkpoint blockade. To test this hypothesis, we evaluated the effect of an orally active, high-affinity CCR2 antagonist, CCX872 (60–62), to slow progression of gliomas when combined with anti-PD-1 therapy. To determine the effect on survival, KR158 glioma-bearing mice were treated with anti-PD-1 and/or CCX872 and followed to humane end point. Vehicle/immunoglobulin G (IgG)-treated and anti-PD-1 monotherapy-treated animals showed no difference in median or durable survival. In contrast, CCX872 monotherapy increased ($P = 0.002$) median survival time (32 d vs. 50 d), while combination treatment resulted in a significant durable survival advantage over vehicle/IgG ($P = 0.001$) and CCX872 single treatment ($P = 0.001$) (Fig. 4*B*). Median survival of 005 GSC tumor-bearing animals was increased (30 vs. 49 d; $P = 0.005$) with combination treatment, although no CCX872 monotherapy effect was observed (Fig. 4*C*).

CCX872 Impedes Invasion of MDSC into Tumors and Prevents Egress from Bone Marrow. Similar to findings in CCR2-deficient mice, flow-cytometric analysis of CCX872-treated KR158-bearing animals revealed a decrease ($P = 0.038$) in the population of $CD45^{hi}/CD11b^+/Ly6C^{hi}$ cells within the tumor microenvironment (Fig. 5*A*). A significant increase ($P = 0.028$) of this population was observed in bone marrow. Analysis of 005 GSC tumor-bearing animals mirrors the results observed with KR158 gliomas, i.e., a significant reduction ($P = 0.015$) in the $Ly6C^{hi}$ cell population within the tumors, and a concomitant increase ($P = 0.028$) of this population in the bone marrow was seen (Fig. 5*B*).

We next investigated the effect of CCX872 treatment on the 3 CCR2- and CX3CR1-expressing subpopulations. KR158 or 005 GSC bearing $CCR2^{RFP/WT}$;$CX3CR1^{GFP/WT}$ mice were treated with either vehicle or CCX872. Immune cell populations were subsequently isolated and subjected to flow-cytometric analysis of CCR2/RFP and CX3CR1/GFP expression, as well as for CD45, CD11b, Ly6C, and Ly6G. Analysis of KR158 tumors revealed a significant decrease ($P = 0.003$) in RFP^+, i.e., $CCR2^+/CX3CR1^-$ cells with CCX872 treatment. Similarly, $CCR2^+/CX3CR1^+$ reported a decrease ($P = 0.032$) with CCX872 treatment (Fig. 5 *C*, *Upper*). Consistent with previous results, CCX872 treatment reduced ($P = 0.004$) $CD45^{hi}/CD11b^+/Ly6C^{hi}$ cells within KR158 tumors (Fig. 5 *C*, *Lower*). Parallel analysis was performed in 005 GSC glioma-bearing animals. A significant reduction of CCR2 single-positive ($P = 0.003$), $CX3CR1^+$ ($P = 0.003$), as well as CCR2/CX3CR1 double-positive ($P = 0.042$) events (Fig. 5 *D*, *Upper*) were observed in tumors from CCX872-treated mice. Analysis of $CD45^{hi}/CD11b^+/Ly6C^{hi}$ cells within 005 GSC tumors also showed a reduction ($P = 0.020$) in $Ly6C^{hi}$ events with CCX872 treatment (Fig. 5 *D*, *Lower*).

CCX872/Anti-PD-1 Combination Therapy Enhances Activation and Reduces Exhaustion of Intratumoral T Cells. The effects of combination therapy on T cell populations in 005 GSC glioma-bearing wild-type (WT) mice were evaluated. Peripheral $CD4^+$ and $CD8^+$ T cell populations in blood (*SI Appendix*, Fig. S6*A*) and lymph nodes (*SI Appendix*, Fig. S6*B*) were not impacted by any of the treatments. A significant increase in tumor-infiltrating $CD45^+/CD3^+/CD4^+$ T cells was noted with combination therapy ($P = 0.044$), while a trend ($P = 0.056$) toward increased percentage of $CD45^+/CD3^+/CD8^+$ T cells was observed (Fig. 6*A*). Neither of the monotherapies produced changes in these tumor-infiltrating T cell populations.

To assess the activation status of tumor-infiltrating T cells, we evaluated IFNγ expression using IFNγ reporter with endogenous poly(A) transcript (GREAT) IFNγ reporter mice, which have YFP under the control of the IFNγ promoter. No significant increase in IFNγ expression was noted with either monotherapy. However, glioma-infiltrating T cells from tumor-bearing mice administered the combination therapy had a significant increase in IFNγ expression (Fig. 6*B*, $P = 008$). Examination of T cell exhaustion markers ($PD\text{-}1^+/Tim3^+$) on $CD4^+$ and $CD8^+$ T cells within tumors derived from all treatment groups determined that only the CCX872/anti-PD-1 combination therapy produced significant reductions of $CD45^+/CD3^+/PD\text{-}1^+/Tim3^+/CD4^+$ (Fig. 6*C*, $P = 0.029$) and $CD45^+/CD3^+/PD\text{-}1^+/Tim3^+/CD8^+$ (Fig. 6*D*, $P = 0.011$) T cells. These data suggest combination therapy results in enhanced tumor infiltration of lymphocytes that are less dysfunctional.

Discussion

Since the inclusion of temozolomide into the standard-of-care regimen for GBM, little progress has been made in the development of effective treatments for this disease. Stagnating survival rates underscore the need for next generation approaches for the treatment of GBM. While immunotherapy-based approaches have been attempted, most clinical trials involving these modalities have failed to report significant outcomes. Elevated levels of MDSCs, both in the peripheral blood and tumor microenvironment of GBM patients, have been described (34, 39). MDSCs are known to potentiate immune suppression in GBM and may contribute to the failure of immune therapies for gliomas (34–40, 42). The exact mechanism by which MDSCs traffic to the tumor is not wholly defined, although evidence supports a role of CCR2 in this process (40). As such, we set out to determine if mice bearing immune-checkpoint inhibitor-resistant gliomas would gain a

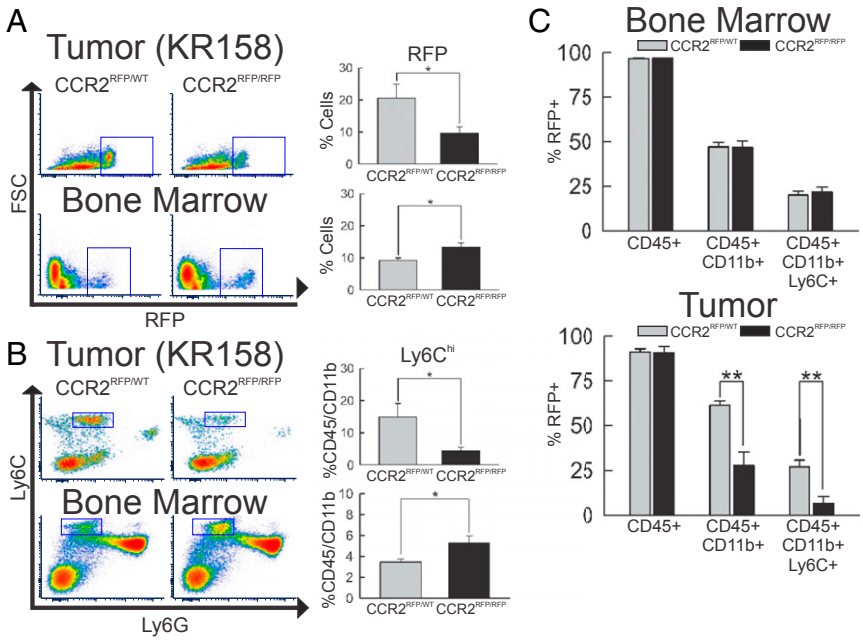

Fig. 3. Impact of Ccr2 deficiency on peripheral and tumor MDSC populations. (*A*) Flow-cytometric analysis of RFP$^+$ events in Ccr2$^{RFP/WT}$ ($n = 6$) vs. Ccr2$^{RFP/RFP}$ ($n = 6$) mice. Population of RFP$^+$ cells within the tumor microenvironment (*Upper*) is reduced ($P = 0.047$) but increased ($P = 0.024$) in bone marrow (*Lower*) of Ccr2-deficient animals. (*B*) Flow-cytometric analysis of CD45$^+$/CD11b$^+$/Ly6C^{hi} events in Ccr2$^{RFP/WT}$ ($n = 5$) vs. Ccr2$^{RFP/RFP}$ ($n = 5$) mice. Population of CD45$^+$/CD11b$^+$/Ly6C^{hi} cells within the tumor microenvironment (*Upper*) was reduced ($P = 0.039$) but increased ($P = 0.020$) in bone marrow (*Lower*) of Ccr2-deficient animals. (*C*) Quantification of percentage of RFP$^+$ cells that are CD45$^+$, CD45$^+$/CD11b$^+$, and CD45$^+$/CD11b$^+$/Ly6C^{hi} within bone marrow (*Upper*) and tumor (*Lower*) in Ccr2$^{RFP/WT}$ ($n = 5$) vs. Ccr2$^{RFP/RFP}$ ($n = 5$) mice. Ratios remain unchanged in bone marrow but show a significant reduction ($P = 0.007$) of CD45$^+$/CD11b$^+$/Ly6C^{hi} cells in tumors of Ccr2$^{RFP/RFP}$ vs. Ccr2$^{RFP/WT}$ mice. Representative plots are shown throughout. *$P < 0.05$; **$P < 0.01$. FSC, forward scatter.

survival advantage with inhibition of CCR2. Indeed, we demonstrate that blocking CCR2 by either gene deletion or pharmacological antagonism is able to unmask efficacy of immune-checkpoint blockade in 2 clinically relevant murine glioma models. Our data suggest that the enhanced survival is a consequence of reduced MDSCs within the glioma microenvironment, a concomitant increase of this cell population within bone marrow, and an increase in functional tumor-infiltrating lymphocytes.

Selection of KR158 and 005 GSC glioma models allowed for evaluation of our proposed treatment paradigm in immune-competent mice that recapitulate many of the features of human GBM (e.g., morphology, lack of hypermutation, and aggressive/invasive growth), and, importantly, immune-checkpoint inhibitor resistance. Nonetheless, the models do present with limitations. First and foremost, human GBM is classically heterogeneous in nature, and use of a single cell line to elicit a glioma does not necessarily recreate that feature. Furthermore, these lines rely on p53 mutation and aberrant RAS signaling to induce tumors, while human GBM typically presents with additional common mutations, including EGFR, IDH, and PDGFRα.

Previous work using the CCR2$^{RFP/WT}$;CX3CR1$^{GFP/WT}$ double-transgenic reporter mouse demonstrated the presence of 3 CCR2- and/or CX3CR1-expressing cell populations in GL261 tumors (63), and our findings extend this observation to more clinically relevant murine models of therapy resistant gliomas. Tumor-associated myeloid (TAM) cell infiltration is an established characteristic of GBM and has a known influence on disease progression, with both resident microglia and bone marrow-derived infiltrating monocytes potentially exerting tumor growth-promoting activities (35, 40, 43, 45, 46, 63, 64). Understanding specific roles of the various myeloid cell subsets in glioma progression will be critical in the development of novel therapeutics that aim to mitigate their protumorigenic effects.

Studies aimed at targeting microglia have been conducted, as increased microglial infiltration in gliomas has been associated with poorer outcomes in patients. Modulation of the chemokine receptor characteristically expressed by microglia, CX3CR1, by our laboratory and others reported modest reductions in survival time with CX3CR1 deficiency in murine models of glioma (43, 45). An indirect effect of CX3CR1 deficiency on the presence of MDSC-like monocytes within CNS tumors and an associated increase of IL1β and the CCR2 ligand, CCL2, has been reported (43). In this study, we identified a CX3CR1$^+$/Ly6C^{lo} that is present within the glioma that may impact response to treatment, as cells with similar phenotype have been linked to treatment resistance in response to anti-VEGFR2 inhibitors (65). Furthermore, Butowski et al. (66) investigated the efficacy of using a colony-stimulating factor 1 receptor (CSF1R) inhibitor as a means to modulate microglia within the GBM tumor microenvironment but found no clinical benefit. This approach of broadly targeting CSFR1-expressing myeloid populations, which include microglia, macrophages, mast cells, and osteoclasts, may limit overall efficacy within the CNS. Additionally, impacting brain-derived microglia and/or myeloid cells after they gain entry into the tumor requires drug penetration of the blood–brain barrier. The approach reported herein may hold value for more specific intervention by antagonizing only the CCR2-expressing subpopulation of myeloid cells. Furthermore, retention of MDSCs in the bone marrow as a consequence of CCR2 disruption does not require drug penetration of the blood brain barrier.

Disruption of CCR2 not only leads to reduced MDSCs within tumors but an associated accumulation of these cells in the bone marrow. A role for CCR2 in mobilization of leukocytes from the bone marrow has been reported previously (48, 67–69), and the mechanism likely involves interactions with another chemokine receptor, CXCR4 (70). The egress of CCR2$^+$ cells from the bone marrow and influx into the tumors may be mediated by any known ligand for CCR2. In addition to CCL2, MCP-3 (CCL7) has been shown to be integral in migration of CCR2$^+$ monocytes out of the bone marrow (48). Expression of CCL2 has been

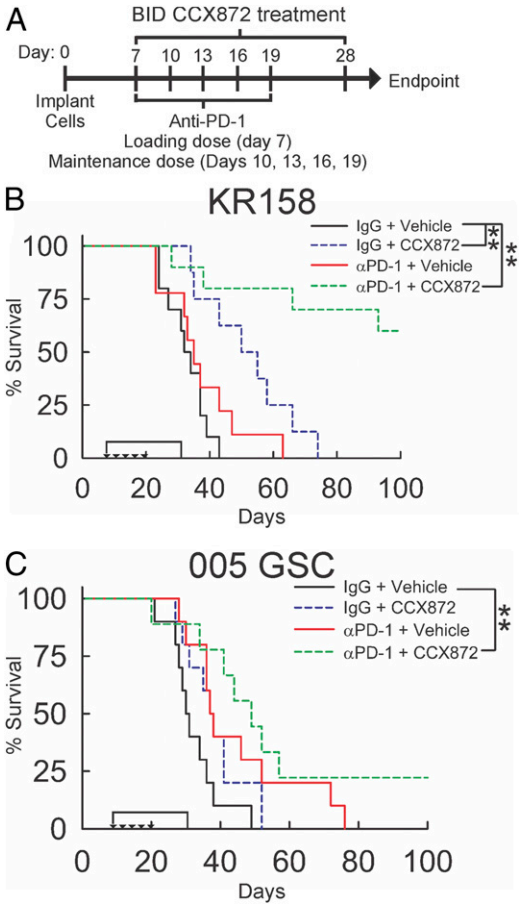

Fig. 4. Effect of combinatorial CCX872/anti-PD-1 treatment on survival of KR158 and 005 GSC glioma-bearing mice. (*A*) Schematic representation of CCX872 and anti-PD-1 treatment schedules. Survival analysis of KR158 (n= 8 to 10) (*B*) and 005 GSC ($n = 8$ to 10) (*C*) tumor-bearing WT mice treated with CCX872 and anti-PD-1. In KR158 glioma-bearing mice, CCX872 increased median survival ($P = 0.002$, 32 vs. 50 d). Combinatorial treatment increased durable survival ($P = 0.001$); 005 GSC-bearing animals had an increase in median survival ($P = 0.005$, 30 vs. 49 d) with combinatorial treatment. Triangles mark anti-PD-1 administration. The bracket indicates CCX872 administration. $^{*}P < 0.05$; $^{**}P < 0.01$.

shown to correlate with survival time in human GBM patients, with patients who exhibit low CCL2 expression surviving longer than individuals expressing high levels of this chemokine (40). This trend was recapitulated in GL261 glioma-bearing mice (47, 63). Considering the heterogeneity in CCL2 expression observed in human patients, the variation in myeloid cell infiltration and survival between KR158 and 005 GSC CCR2 antagonist-treated gliomas noted in our study may reflect differences in CCR2 ligand expression between the 2 models. Nonetheless, given the redundancy in ligands for CCR2, approaches targeting either CCL2 or CCL7 individually may not be fruitful (71), warranting our approach of directly targeting CCR2.

While CCR2 deficiency did not impact overall survival of KR158 glioma-bearing mice, a CCX872 monotherapy was observed, albeit only in the KR158 model and not in 005 GSC tumor-bearing animals. Possibilities for this discrepancy include expression of CCR2 on implanted KR158 cells that would be a target of CCX872. Availability of highly specific anti-murine CCR2 antibodies limited a direct assessment of this potential mechanism. Compensatory mechanism(s) as a consequence of global germline loss of CCR2 are known and may not arise similarly from acute pharmacologic antagonism of this receptor, thereby leading to distinct outcomes. Lack of ligand, e.g., CCL2, internalization has been shown in mice devoid of CCR2, with concomitant increases in levels of circulating CCL2 (72). Elevated CCL2 may then bind and activate other chemokine receptors, namely CCR1 or CCR11. Additionally, CCL7 may be similarly affected and is known to bind CCR1 and CCR3 in addition to CCR2. These compensatory changes may not be sufficiently triggered by short-term pharmacologic blockade of CCR2.

MDSCs have potential for wide-ranging impacts on T cell activation and proliferation (73). The effects are exerted via an array of mechanisms including arginase-1/inducible nitric oxide synthase (Arg-1/iNOS) expression (74, 75), reactive oxygen species production (76, 77), and recruitment of T-regulatory cells (78). Studies have suggested that infiltration of MDSCs into the GBM microenvironment is associated with a reduction in infiltrating lymphocytes (35). Additionally, it has been reported that PD-1 blockade increases tumor T cell infiltration in models of melanoma and colon cancer via an IFN-γ–dependent mechanism (79). In the models used herein, CCR2 antagonist monotherapy had no impact on intratumoral T cell populations, while PD-1 blockade alone only marginally increased $CD8^+$ T cells, although not significantly. However, elevated populations of both $CD4^+$ and $CD8^+$ T cells within 005 GSC tumors were observed with combination treatment. The increased T cell populations may be due to increased infiltration or reduced T cell death within tumors. Exhaustion has been shown to promote T cell apoptosis via the PD-1/PD-L1 axis and therefore may contribute to loss of T cells at the tumor site (80). Using PD-1/Tim3 double expression on $CD4^+$ or $CD8^+$ T cells as a marker for exhaustion (81, 82), we determined that only the combination therapy was able to reduce the population of exhausted T cells within the tumor. Given that anti-PD-1 treatment alone did not enhance survival in either model, and was able to only marginally increase intratumoral T cell population, these data may suggest the reduced exhaustion with combination therapy may be driving improvement in overall survival. Recently published clinical research has suggested that altering the timing of delivery, particularly as a neoadjuvant intervention, of anti-PD-1 agents improves efficacy of immune-checkpoint inhibitors for GBM patients (13, 14). In light of these results, future experiments should include investigation into the timing of administration of PD-1 blockade in combination with CCR2 antagonism. For instance, preconditioning the immune-suppressed tumor microenvironment via neoadjuvant CCR2 antagonism of MDSCs may further enhance an anti-PD-1 effect on infiltrating lymphocytes, yielding an even greater survival benefit with this combinatorial approach.

To summarize, our data show that CCR2 deficiency augments anti-PD-1 treatment and unmasks a survival advantage in glioma-bearing mice. These results are recapitulated with CCR2 antagonism in mice bearing either KR158 or 005 GSC murine glioma models, supporting the hypothesis that CCR2 antagonism, when delivered in conjunction with anti-PD-1, may be a viable approach for the treatment of human gliomas. The use of anti-PD-1–resistant syngeneic murine models enhances the translational value of this study as compared to others that have relied on immune-deficient mice or anti-PD-1–responsive glioma models. Furthermore, the use of CCX872 (currently in Phase 1b clinical trials for the treatment of pancreatic cancer [ClinicalTrials.gov Identifier NCT02345408]), in combination with a clinically available treatment (PD-1 blockade) would allow for expedited translation of these preclinical results into early-phase human clinical trials.

Materials and Methods

Cell Culture. KR158 glioma cells were maintained in Dulbecco modified Eagle medium (DMEM) supplemented with 10% heat-inactivated fetal bovine

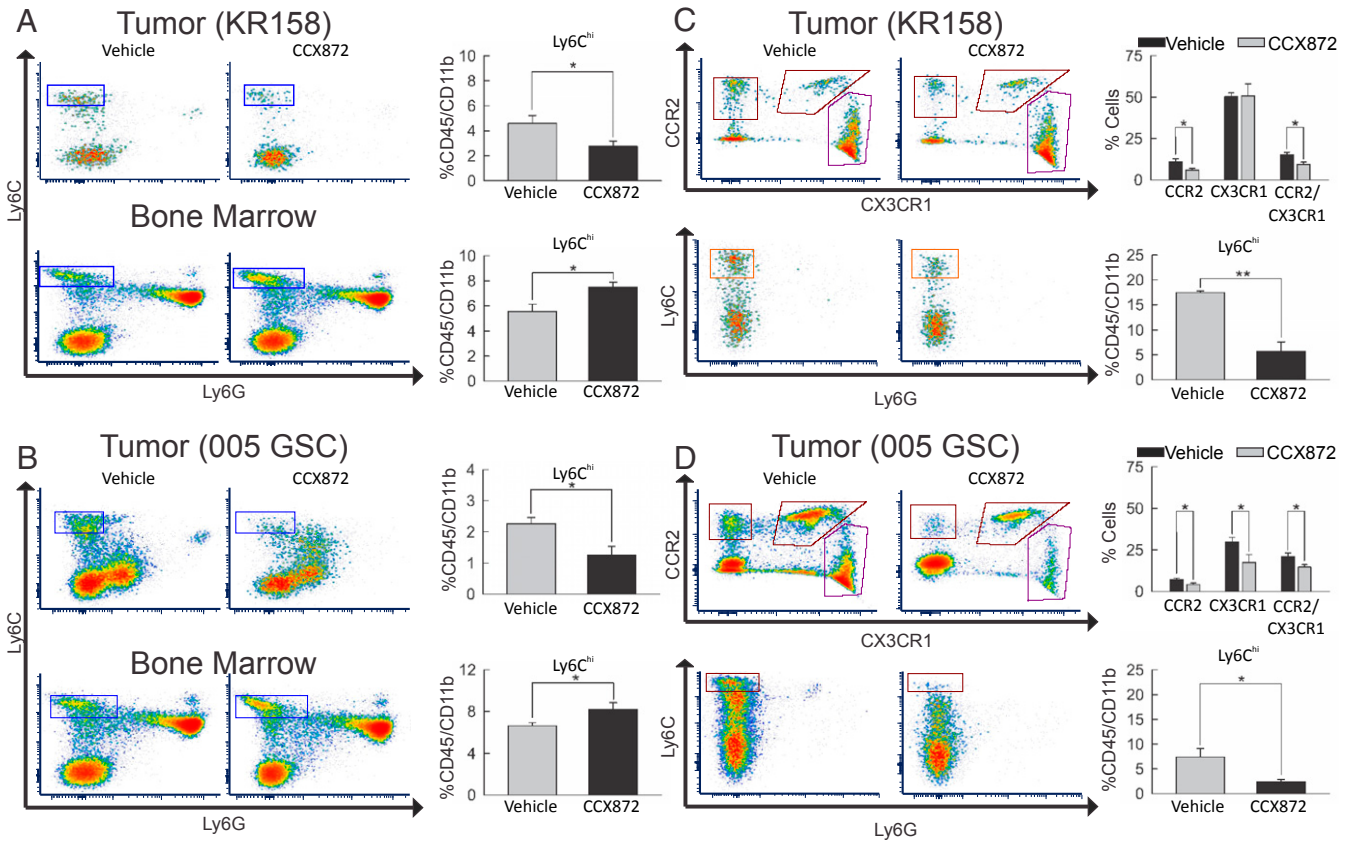

Fig. 5. Impact of combinatorial CCX872/anti-PD-1 treatment on peripheral and tumor myeloid cell populations. (*A*) Flow-cytometric analysis of Ly6C$^+$ vs. Ly6G$^+$ events in KR158 tumor isolates (*Upper*) and bone marrow cell populations (*Lower*) from vehicle-treated ($n = 6$) and CCX872-treated ($n = 6$) animals. Drug treatment resulted in a reduction ($P = 0.038$) of Ly6C^{hi} events within tumors and an increase ($P = 0.028$) in bone marrow. (*B*) Flow-cytometric analysis of Ly6C$^+$ vs. Ly6G$^+$ events in 005 GSC tumor isolates (*Upper*) and bone marrow cell populations (*Lower*) from vehicle-treated ($n = 6$) and CCX872-treated ($n = 5$) animals. Drug treatment resulted in a reduction ($P = 0.015$) in Ly6C^{hi} events within tumors and an increase ($P = 0.028$) in bone marrow. (*C*) Flow-cytometric analysis of tumor isolates from KR158 tumor-bearing Ccr2$^{RFP/WT}$/Cx3cr1$^{GFP/WT}$ mice depicting CCR2$^+$ vs. CX3CR1$^+$ (*Upper*) and Ly6C$^+$ vs. Ly6G$^+$ events (*Lower*) from vehicle-treated ($n = 5$) and CCX872-treated ($n = 7$) animals. Drug treatment resulted in a significant reduction of CCR2$^+$ ($P = 0.024$) and CCR2$^+$/CX3CR1$^+$ ($P = 0.032$) events. The lower graphs report a reduction ($P = 0.004$) in Ly6C^{hi} events within tumors. (*D*) Flow-cytometric analysis of tumor isolates from 005 GSC tumor-bearing Ccr2$^{RFP/WT}$/Cx3cr1$^{GFP/WT}$ mice depicting CCR2$^+$ vs. CX3CR1$^+$ (*Upper*) and Ly6C$^+$ vs. Ly6G$^+$ events (*Lower*) from vehicle-treated ($n = 6$) and CCX872-treated ($n = 6$) animals. Drug treatment resulted in a reduction of CCR2$^+$ ($P = 0.003$), CX3CR1$^+$ ($P = 0.003$), and CCR2$^+$/CX3CR1$^+$ ($P = 0.0419$) events. The lower graphs report a reduction ($P = 0.020$) in Ly6C^{hi} events within tumors. Representative plots are shown throughout. *$P < 0.05$; **$P < 0.01$.

serum (FBS) and 1% penicillin–streptomycin; 005 GSC glioma cells were cultured as neurospheres in serum-free Advanced DMEM/F12 medium supplemented with 2 mM L-glutamine, 1% N2 supplement, 2 mg/mL heparin, 0.5% penicillin–streptomycin, 20 ng/mL recombinant human EGF, and 20 ng/mL recombinant human FGF-basic. GL261 glioma cells were cultured in Roswell Park Memorial Institute (RPMI)-1640 supplemented with 10% FBS, 4 mM L-glutamine, and 1% penicillin–streptomycin. All cells were grown in a humidified incubator at 37 °C with 5% CO_2. DMEM, Advanced DMEM/F12, N2 supplement, EGF, bFGF, L-glutamine, and antibiotics were obtained from Gibco-BRL (Invitrogen). Heparin was purchased from Sigma-Aldrich. FBS was from HyClone (Thermo Scientific).

Animals. WT C57BL/6, Ccr2-deficient (Ccr2$^{RFP/RFP}$[B6.129(Cg)-Ccr2$^{tm2.1Ifc}$/J]), and Cx3cr1-deficient (Cx3cr1$^{GFP/GFP}$[B6.129P-Cx3cr1^{tm1Litt}/J]) mice were obtained from The Jackson Laboratory. IFNγ reporter mice (GREAT) were from The Jackson Laboratory. Ccr2$^{RFP/WT}$/Cx3cr1$^{GFP/WT}$ mice (double knock-in) were generated via in-house breeding. All procedures involving animal housing and surgical protocols were followed according to the guidelines of the University of Florida Institutional Animal Care and Use Committee.

Intracranial Injection of GBM Cells. Animals were anesthetized using isoflurane and administered analgesia prior to cell injection. While under anesthesia, the surgical site was prepared, a 2- to 3-mm incision was made at the midline of the skull, and a small burr hole was drilled 1-mm posterior and 2-mm lateral from bregma. KR158 glioma (7.5×10^4), 005 GSC glioma cells (5×10^4), or GL261 glioma cells (0.75 to 1×10^5) in a total volume not exceeding 2 μL were injected 3-mm deep into the right cerebral hemisphere. The surgical site was closed via suture, and the animal was placed into a warm cage for postsurgical monitoring.

Drug Treatments. CCX872 was delivered for 21 d, beginning on day 7 after tumor cell injection, by oral gavage at a dose of 90 mg/kg, twice daily. Animals also received either anti-PD-1 (catalog no. BE0146, clone RMP1-14; BioXcell) or nonimmune IgG (catalog no. BE0089, clone 2A; BioXcell) treatment injected intraperitoneally alone or in combination with CCX872, every third day beginning on 7 d after implantation, for a total of 5 doses (loading dose of 500 μg/100 μL, followed by 4 doses of 200 μg/100 μL). A control group of mice was treated in parallel to drug administration with vehicle and/or nonimmune IgG. The number of mice used in each treated group is indicated within the figure legends.

Kaplan–Meier Analysis for Survival. For Kaplan–Meier survival analysis, percentages of surviving mice in the various groups were recorded daily after either KR158 or 005 GSC glioma cell implantation, until end point or 100 to 120 d, at which time, all remaining animals were euthanized. Humane end point was defined by a lack of physical activity, body weight reduction >15%, loss of righting response, body score <2, onset of seizures, or signs of pain/distress. Log-rank test was used to determine significance between the experimental groups.

Bone Marrow Imaging. Mice were euthanized, after which, femurs were removed and fixed in 4% paraformaldehyde (PFA) at 4 °C for 3 d with

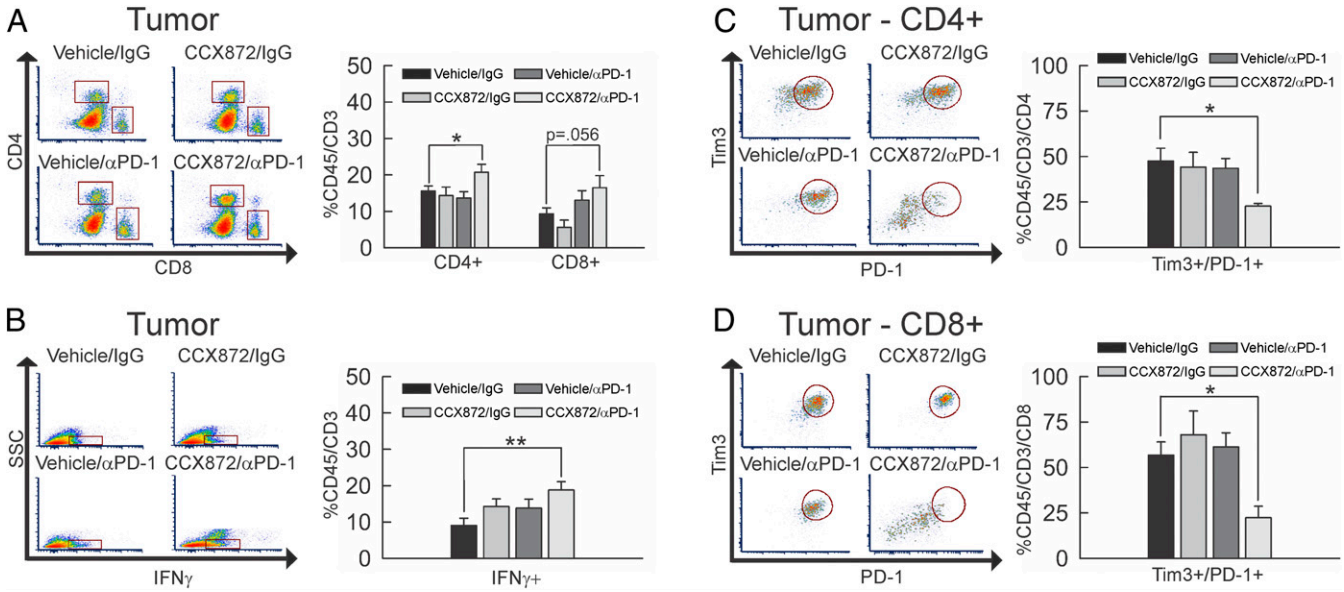

Fig. 6. Impact of combinatorial CCX872/anti-PD-1 treatment on $CD4^+$ and $CD8^+$ T cells. (*A*) Flow-cytometric analysis of $CD45^+/CD3^+/CD4^+$ and $CD8^+$ events within tumor extracts from vehicle/IgG-treated ($n = 7$), CCX872/IgG-treated ($n = 4$), vehicle/anti-PD-1–treated ($n = 6$), or CCX872/anti-PD-1–treated ($n = 4$) 005 GSC glioma-bearing mice. The population of $CD45^+/CD3^+/CD4^+$ cells (upper square) was significantly increased ($P = 0.044$) with combination CCX872/anti-PD-1 treatment as compared to vehicle/IgG, while the $CD45^+/CD3^+/CD8^+$ population (lower square) trended toward increase ($P = 0.056$) between the same groups. (*B*) Flow-cytometric analysis of side scatter (SSC) vs. $CD45^+/CD3^+/IFN\gamma^+$ events (denoted by square) within tumor extracts from vehicle/IgG-treated ($n = 7$), CCX872/IgG-treated ($n = 4$), vehicle/anti-PD-1–treated ($n = 5$), or CCX872/anti-PD-1–treated ($n = 6$) 005 GSC glioma-bearing mice. The population of $CD45^+/CD3^+/IFN\gamma^+$ cells was significantly increased ($P = 0.008$) with combination CCX872/anti-PD-1 treatment as compared to vehicle/IgG. (*C* and *D*) Flow-cytometric analysis of $CD45^+/CD3^+/PD\text{-}1^+/Tim3^+/CD4^+$ (*C*) and $CD8^+$ (*D*) events within tumor extracts from vehicle/IgG-treated ($n = 7$), CCX872/IgG-treated ($n = 4$), vehicle/anti-PD-1–treated ($n = 6$), or CCX872/anti-PD-1–treated ($n = 4$) 005 GSC glioma-bearing mice. The population of $CD45^+/CD3^+/PD\text{-}1^+/Tim3^+/CD4^+$ cells (circled population) was significantly decreased ($P = 0.029$) with combination CCX872/anti-PD-1 treatment as compared to vehicle/IgG. The population of $CD45^+/CD3^+/PD\text{-}1^+/Tim3^+/CD8^+$ cells (circled population) also decreased ($P = 0.011$) between the same groups. Representative plots are shown throughout. $*P < 0.05$; $**P < 0.01$.

constant agitation. Following fixation, femurs were decalcified using 14% ethylenediaminetetraacetic acid (EDTA)/9% ammonium hydroxide (wt/vol; pH 7.1) decalcifying solution at 4 °C for 3 d with constant agitation, changing solution every 24 h. Bones were then washed in PBS for 2 h and then soaked in 30% sucrose at 4 °C overnight with constant agitation. Bones were then embedded in optimal cutting temperature medium, sectioned, and analyzed by fluorescent microscopy.

Immunohistochemistry. For immunohistochemistry, brain sections from $Ccr2^{RFP/WT}$ and $Ccr2^{RFP/RFP}$ mice were first permeabilized with 0.5% Triton X-100 for 15 min at room temperature, followed by heating slides (immersed in a boiling water bath for 25 min) in a buffer containing 10 mM sodium citrate, 0.05% Tween 20, pH 6.0. Slides were then cooled to room temperature for 20 min, washed with PBS 3 times, and blocked with 10% goat serum in PBS for 30 min. The sections were incubated in primary antibodies at 4 °C overnight. Antibodies used are listed in *SI Appendix*, Table S1. The following day, sections were washed 3 times with PBS and incubated subsequently in goat anti-rat Alexa 594 (dilution 1:1,000; BD Pharmingen). The sections were then washed 3 times with PBS, counterstained with 4′,6-diamidino-2-phenylindole, and imaged by fluorescent microscopy.

Flow Cytometry. Mice were euthanized using CO_2 asphyxiation at experimental end point. Following euthanasia, the spleen and femur were removed and placed in PBS. The animal was subsequently perfused with 0.9% saline via cardiac puncture, and the brain removed. Bone marrow was extracted by flushing with PBS using a 25-gauge needle. Splenocytes were liberated by fracturing the organ capsule between glass slides and rinsing with fluorescence-activated cell-sorter washing buffer (PBS and 1% FBS) (FACS), followed by needle puncture with an 18-gauge needle. Splenocytes were then collected by centrifugation (4 °C, 380 × *g*, 5 min), resuspended in FACS, and passed through a 50-μm cell strainer. Splenocytes and bone marrow samples were then centrifuged (4 °C, 380 × *g*, 5 min), resuspended in ACK lysis buffer (Gibco, Invitrogen), and incubated for 1.5 min at room temperature (Splenocytes) or 10 min (bone marrow) at 4 °C. At the end of incubation, lysis was halted using 9 mL of FACS buffer. Cells were then centrifuged (4 °C, 380 × *g*, 5 min), resuspended in PBS, and collected in 1.5-mL microcentrifuge tubes. Tumors were then excised from brains and minced using a razor blade. Tissue was suspended in 4 °C Accumax dissociation solution (Innovative Cell Technologies) and incubated at 37 °C for 5 min, followed by 5 min of agitation at room temperature. Cells were then passed through a 70-μm strainer, centrifuged (4 °C, 380 × *g*, 5 min), and resuspended in 4 mL of 70% Percoll (70% Percoll and 1% PBS in RPMI-1640 cell medium). This cell suspension was then gently layered beneath a 37% Percoll layer (4 mL, 37% Percoll and 1% PBS in RPMI-1640 cell medium) using an 18-gauge needle and centrifuged (30 min, room temperature, 500 × *g*), and the interface was removed and placed into a 1.5-mL microcentrifuge tube. All cells were then washed with ice-cold PBS, counted by trypan blue exclusion, aliquoted to 1×10^6 cells/100 μL, and blocked using 0.5-μg anti-mouse CD16/32 (101320; Biolegend) for 30 min at 4 °C. Subsequently, cells were stained for markers of interest (see *SI Appendix*, Table S1 for antibodies used) for 30 min at 4 °C. Cells were then washed twice in ice-cold PBS and either fixed in 4% PFA for 30 min and resuspended in FACS buffer or left unfixed if isolated from reporter mice. Intracellular staining of FoxP3 was carried out according to manufacturer instructions using the eBioscience FOXP3/Transcription Factor Staining Buffer Set (no. 00-5523-00; Invitrogen). Stained samples were analyzed using single-color compensation on either a BD LSR Fortessa flow cytometer (BD Biosciences) or a Sony SP6800 spectral analyzer and quantified using FCS Express software (De Novo Software).

Statistical Analysis. Student *t* test was performed in SigmaPlot (SigmaPlot) as indicated in the results. *P* values were calculated using Student *t* test with 2-tailed distribution. Survival data were subjected to log-rank test using GraphPad Prism 5 software (GraphPad Software) to determine statistically significant differences between groups. A *P* value of <0.05 was considered significant and is indicated by symbols depicted in the figures and figure legends.

Data Availability. All data are included in the main text and *SI Appendix*.

ACKNOWLEDGMENTS. We thank Andria Doty for assistance with flow-cytometry analysis. The research reported in this study was funded by the Florida Center for Brain Tumor Research, Accelerate Brain Cancer Cures (J.K.H.); the American Association of Cancer Research (M.D.); and National Institutes of Health Grant R01NS108781 (to J.K.H. and D.A.M.). R.K.J. is a recipient of grants from the National Cancer Institute (R35CA197743) and National Foundation for Cancer Research.

1. R. Stupp *et al*.; European Organisation for Research and Treatment of Cancer Brain Tumor and Radiotherapy Groups; National Cancer Institute of Canada Clinical Trials Group, Radiotherapy plus concomitant and adjuvant temozolomide for glioblastoma. *N. Engl. J. Med.* **352**, 987–996 (2005).
2. F. B. Furnari *et al*., Malignant astrocytic glioma: Genetics, biology, and paths to treatment. *Genes Dev.* **21**, 2683–2710 (2007).
3. P. Y. Wen, S. Kesari, Malignant gliomas in adults. *N. Engl. J. Med.* **359**, 492–507 (2008).
4. F. Johansson Swartling, Identifying candidate genes involved in brain tumor formation. *Ups. J. Med. Sci.* **113**, 1–38 (2008).
5. H. Colman, K. Aldape, Molecular predictors in glioblastoma: Toward personalized therapy. *Arch. Neurol.* **65**, 877–883 (2008).
6. S. Mittal, S. Pradhan, T. Srivastava, Recent advances in targeted therapy for glioblastoma. *Expert Rev. Neurother.* **15**, 935–946 (2015).
7. J. H. Kang, C. Adamson, Novel chemotherapeutics and other therapies for treating high-grade glioma. *Expert Opin. Investig. Drugs* **24**, 1361–1379 (2015).
8. M. D. Prados *et al*., Toward precision medicine in glioblastoma: The promise and the challenges. *Neuro Oncol.* **17**, 1051–1063 (2015).
9. R. Stupp *et al*.; European Organisation for Research and Treatment of Cancer Brain Tumour and Radiation Oncology Groups; National Cancer Institute of Canada Clinical Trials Group, Effects of radiotherapy with concomitant and adjuvant temozolomide versus radiotherapy alone on survival in glioblastoma in a randomised phase III study: 5-year analysis of the EORTC-NCIC trial. *Lancet Oncol.* **10**, 459–466 (2009).
10. M. Preusser, M. Lim, D. A. Hafler, D. A. Reardon, J. H. Sampson, Prospects of immune checkpoint modulators in the treatment of glioblastoma. *Nat. Rev. Neurol.* **11**, 504–514 (2015).
11. K. K. Chow, W. Hara, M. Lim, G. Li, Combining immunotherapy with radiation for the treatment of glioblastoma. *J. Neuro Oncol.* **123**, 459–464 (2015).
12. M. Lim, Y. Xia, C. Bettegowda, M. Weller, Current state of immunotherapy for glioblastoma. *Nat. Rev. Clin. Oncol.* **15**, 422–442 (2018).
13. T. F. Cloughesy *et al*., Neoadjuvant anti-PD-1 immunotherapy promotes a survival benefit with intratumoral and systemic immune responses in recurrent glioblastoma. *Nat. Med.* **25**, 477–486 (2019).
14. K. A. Schalper *et al*., Neoadjuvant nivolumab modifies the tumor immune microenvironment in resectable glioblastoma. *Nat. Med.* **25**, 470–476 (2019).
15. D. A. Reardon *et al*., OS10.3 randomized phase 3 study evaluating the efficacy and safety of nivolumab vs bevacizumab in patients with recurrent glioblastoma: CheckMate 143. *Neuro Oncol.* **19** (suppl. 3), iii21 (2017).
16. P. Chongsathidkiet *et al*., Sequestration of T cells in bone marrow in the setting of glioblastoma and other intracranial tumors. *Nat. Med.* **24**, 1459–1468 (2018).
17. M. A. Postow *et al*., Nivolumab and ipilimumab versus ipilimumab in untreated melanoma. *N. Engl. J. Med.* **372**, 2006–2017 (2015).
18. C. Robert *et al*.; KEYNOTE-006 investigators, Pembrolizumab versus ipilimumab in advanced melanoma. *N. Engl. J. Med.* **372**, 2521–2532 (2015).
19. J. Brahmer *et al*., Nivolumab versus docetaxel in advanced squamous-cell non-small-cell lung cancer. *N. Engl. J. Med.* **373**, 123–135 (2015).
20. F. Kawakami *et al*., Programmed cell death ligand 1 and tumor-infiltrating lymphocyte status in patients with renal cell carcinoma and sarcomatoid dedifferentiation. *Cancer* **123**, 4823–4831 (2017).
21. J. Duraiswamy, K. M. Kaluza, G. J. Freeman, G. Coukos, Dual blockade of PD-1 and CTLA-4 combined with tumor vaccine effectively restores T-cell rejection function in tumors. *Cancer Res.* **73**, 3591–3603 (2013).
22. G. Li *et al*., Successful chemoimmunotherapy against hepatocellular cancer in a novel murine model. *J. Hepatol.* **66**, 75–85 (2017).
23. H. Mamdani, H. Wu, B. H. O'Neil, A. Sehdev, Excellent response to anti-PD-1 therapy in a patient with hepatocellular carcinoma: Case report and review of literature. *Discov. Med.* **23**, 331–336 (2017).
24. J. Han, Y. Hong, Y. S. Lee, PD-L1 expression and combined status of PD-L1/PD-1-positive tumor infiltrating mononuclear cell density predict prognosis in glioblastoma patients. *J. Pathol. Transl. Med.* **51**, 40–48 (2017).
25. E. K. Nduom *et al*., PD-L1 expression and prognostic impact in glioblastoma. *Neuro Oncol.* **18**, 195–205 (2016).
26. A. S. Berghoff *et al*., Programmed death ligand 1 expression and tumor-infiltrating lymphocytes in glioblastoma. *Neuro Oncol.* **17**, 1064–1075 (2015).
27. E. Bouffet *et al*., Immune checkpoint inhibition for hypermutant glioblastoma multiforme resulting from germline biallelic mismatch repair deficiency. *J. Clin. Oncol.* **34**, 2206–2211 (2016).
28. D. A. Wainwright *et al*., Durable therapeutic efficacy utilizing combinatorial blockade against IDO, CTLA-4, and PD-L1 in mice with brain tumors. *Clin. Cancer Res.* **20**, 5290–5301 (2014).
29. J. Zeng *et al*., Anti-PD-1 blockade and stereotactic radiation produce long-term survival in mice with intracranial gliomas. *Int. J. Radiat. Oncol. Biol. Phys.* **86**, 343–349 (2013).
30. D. A. Reardon *et al*., Glioblastoma eradication following immune checkpoint blockade in an orthotopic, immunocompetent model. *Cancer Immunol. Res.* **4**, 124–135 (2016).
31. J. E. Kim *et al*., Combination therapy with anti-PD-1, anti-TIM-3, and focal radiation results in regression of murine gliomas. *Clin. Cancer Res.* **23**, 124–136 (2017).
32. J. P. Antonios *et al*., Immunosuppressive tumor-infiltrating myeloid cells mediate adaptive immune resistance via a PD-1/PD-L1 mechanism in glioblastoma. *Neuro Oncol.* **19**, 796–807 (2017).
33. T. J. Alban *et al*., Global immune fingerprinting in glioblastoma patient peripheral blood reveals immune-suppression signatures associated with prognosis. *JCI Insight* **3**, 122264 (2018).
34. B. Raychaudhuri *et al*., Myeloid-derived suppressor cell accumulation and function in patients with newly diagnosed glioblastoma. *Neuro Oncol.* **13**, 591–599 (2011).
35. B. Raychaudhuri *et al*., Myeloid derived suppressor cell infiltration of murine and human gliomas is associated with reduction of tumor infiltrating lymphocytes. *J. Neuro Oncol.* **122**, 293–301 (2015).
36. G. Kohanbash *et al*., GM-CSF promotes the immunosuppressive activity of glioma-infiltrating myeloid cells through interleukin-4 receptor-α. *Cancer Res.* **73**, 6413–6423 (2013).
37. M. Prosniak *et al*., Glioma grade is associated with the accumulation and activity of cells bearing M2 monocyte markers. *Clin. Cancer Res.* **19**, 3776–3786 (2013).
38. M. Chae *et al*., Increasing glioma-associated monocytes leads to increased intratumoral and systemic myeloid-derived suppressor cells in a murine model. *Neuro Oncol.* **17**, 978–991 (2015).
39. P. R. Gielen *et al*., Increase in both CD14-positive and CD15-positive myeloid-derived suppressor cell subpopulations in the blood of patients with glioma but predominance of CD15-positive myeloid-derived suppressor cells in glioma tissue. *J. Neuropathol. Exp. Neurol.* **74**, 390–400 (2015).
40. A. L. Chang *et al*., CCL2 produced by the glioma microenvironment is essential for the recruitment of regulatory T cells and myeloid-derived suppressor cells. *Cancer Res.* **76**, 5671–5682 (2016).
41. B. Otvos *et al*., Cancer stem cell-secreted macrophage migration inhibitory factor stimulates myeloid derived suppressor cell function and facilitates glioblastoma immune evasion. *Stem Cells* **34**, 2026–2039 (2016).
42. M. Platten *et al*., Monocyte chemoattractant protein-1 increases microglial infiltration and aggressiveness of gliomas. *Ann. Neurol.* **54**, 388–392 (2003).
43. X. Feng *et al*., Loss of CX3CR1 increases accumulation of inflammatory monocytes and promotes gliomagenesis. *Oncotarget* **6**, 15077–15094 (2015).
44. J. Cai *et al*., Identification of a 6-cytokine prognostic signature in patients with primary glioblastoma harboring M2 microglia/macrophage phenotype relevance. *PLoS One* **10**, e0126022 (2015).
45. C. Liu, D. Luo, W. J. Streit, J. K. Harrison, CX3CL1 and CX3CR1 in the GL261 murine model of glioma: CX3CR1 deficiency does not impact tumor growth or infiltration of microglia and lymphocytes. *J. Neuroimmunol.* **198**, 98–105 (2008).
46. J. Zhang *et al*., A dialog between glioma and microglia that promotes tumor invasiveness through the CCL2/CCR2/interleukin-6 axis. *Carcinogenesis* **33**, 312–319 (2012).
47. X. Zhu, M. Fujita, L. A. Snyder, H. Okada, Systemic delivery of neutralizing antibody targeting CCL2 for glioma therapy. *J. Neuro Oncol.* **104**, 83–92 (2011).
48. C. L. Tsou *et al*., Critical roles for CCR2 and MCP-3 in monocyte mobilization from bone marrow and recruitment to inflammatory sites. *J. Clin. Invest.* **117**, 902–909 (2007).
49. M. Okada *et al*., Tumor-associated macrophage/microglia infiltration in human gliomas is correlated with MCP-3, but not MCP-1. *Int. J. Oncol.* **34**, 1621–1627 (2009).
50. A. M. Lesokhin *et al*., Monocytic CCR2(+) myeloid-derived suppressor cells promote immune escape by limiting activated CD8 T-cell infiltration into the tumor microenvironment. *Cancer Res.* **72**, 876–886 (2012).
51. R. B. Holmgaard, D. Zamarin, A. Lesokhin, T. Merghoub, J. D. Wolchok, Targeting myeloid-derived suppressor cells with colony stimulating factor-1 receptor blockade can reverse immune resistance to immunotherapy in indoleamine 2,3-dioxygenase-expressing tumors. *EBioMedicine* **6**, 50–58 (2016).
52. I. M. Stromnes *et al*., Targeted depletion of an MDSC subset unmasks pancreatic ductal adenocarcinoma to adaptive immunity. *Gut* **63**, 1769–1781 (2014).
53. M. K. Srivastava *et al*., Targeting myeloid-derived suppressor cells augments antitumor activity against lung cancer. *ImmunoTargets Ther.* **2012**, 7–12 (2012).
54. J. Yu *et al*., Myeloid-derived suppressor cells suppress antitumor immune responses through IDO expression and correlate with lymph node metastasis in patients with breast cancer. *J. Immunol.* **190**, 3783–3797 (2013).
55. J. Vincent *et al*., 5-Fluorouracil selectively kills tumor-associated myeloid-derived suppressor cells resulting in enhanced T cell-dependent antitumor immunity. *Cancer Res.* **70**, 3052–3061 (2010).
56. T. Marumoto *et al*., Development of a novel mouse glioma model using lentiviral vectors. *Nat. Med.* **15**, 110–116 (2009).
57. T. A. Cheema *et al*., Multifaceted oncolytic virus therapy for glioblastoma in an immunocompetent cancer stem cell model. *Proc. Natl. Acad. Sci. U.S.A.* **110**, 12006–12011 (2013).
58. D. Saha, R. L. Martuza, S. D. Rabkin, Macrophage polarization contributes to glioblastoma eradication by combination immunovirotherapy and immune checkpoint blockade. *Cancer Cell* **32**, 253–267.e5 (2017).
59. B. Molon *et al*., Chemokine nitration prevents intratumoral infiltration of antigen-specific T cells. *J. Exp. Med.* **208**, 1949–1962 (2011).
60. J. M. Morganti *et al*., CCR2 antagonism alters brain macrophage polarization and ameliorates cognitive dysfunction induced by traumatic brain injury. *J. Neurosci.* **35**, 748–760 (2015).

61. R. Parker *et al*., CC chemokine receptor 2 promotes recruitment of myeloid cells associated with insulin resistance in nonalcoholic fatty liver disease. *Am. J. Physiol. Gastrointest. Liver Physiol.* **314**, G483–G493 (2018).
62. Z. Miao *et al*., CCR2 antagonism leads to marked reduction in proteinuria and glomerular injury in murine models of focal segmental glomerulosclerosis (FSGS). *PLoS One* **13**, e0192405 (2018).
63. Z. Chen *et al*., Cellular and molecular identity of tumor-associated macrophages in glioblastoma. *Cancer Res.* **77**, 2266–2278 (2017).
64. G. Hutter *et al*., Microglia are effector cells of CD47-SIRPα antiphagocytic axis disruption against glioblastoma. *Proc. Natl. Acad. Sci. U.S.A.* **116**, 997–1006 (2019).
65. K. Jung *et al*., Ly6Clo monocytes drive immunosuppression and confer resistance to anti-VEGFR2 cancer therapy. *J. Clin. Invest.* **127**, 3039–3051 (2017).
66. N. Butowski *et al*., Orally administered colony stimulating factor 1 receptor inhibitor PLX3397 in recurrent glioblastoma: An Ivy Foundation Early Phase Clinical Trials Consortium phase II study. *Neuro Oncol.* **18**, 557–564 (2016).
67. N. Fujimura *et al*., CCR2 inhibition sequesters multiple subsets of leukocytes in the bone marrow. *Sci. Rep.* **5**, 11664 (2015).
68. N. V. Serbina, E. G. Pamer, Monocyte emigration from bone marrow during bacterial infection requires signals mediated by chemokine receptor CCR2. *Nat. Immunol.* **7**, 311–317 (2006).
69. D. R. Engel *et al*., CCR2 mediates homeostatic and inflammatory release of Gr1(high) monocytes from the bone marrow, but is dispensable for bladder infiltration in bacterial urinary tract infection. *J. Immunol.* **181**, 5579–5586 (2008).
70. H. Jung, D. S. Mithal, J. E. Park, R. J. Miller, Localized CCR2 activation in the bone marrow niche mobilizes monocytes by desensitizing CXCR4. *PLoS One* **10**, e0128387 (2015).
71. S. Y. Lim, A. E. Yuzhalin, A. N. Gordon-Weeks, R. J. Muschel, Targeting the CCL2-CCR2 signaling axis in cancer metastasis. *Oncotarget* **7**, 28697–28710 (2016).
72. A. E. Cardona *et al*., Scavenging roles of chemokine receptors: Chemokine receptor deficiency is associated with increased levels of ligand in circulation and tissues. *Blood* **112**, 256–263 (2008).
73. D. I. Gabrilovich, S. Nagaraj, Myeloid-derived suppressor cells as regulators of the immune system. *Nat. Rev. Immunol.* **9**, 162–174 (2009).
74. C. D. Mills, J. Shearer, R. Evans, M. D. Caldwell, Macrophage arginine metabolism and the inhibition or stimulation of cancer. *J. Immunol.* **149**, 2709–2714 (1992).
75. S. A. Kusmartsev, Y. Li, S. H. Chen, Gr-1+ myeloid cells derived from tumor-bearing mice inhibit primary T cell activation induced through CD3/CD28 costimulation. *J. Immunol.* **165**, 779–785 (2000).
76. C. A. Corzo *et al*., Mechanism regulating reactive oxygen species in tumor-induced myeloid-derived suppressor cells. *J. Immunol.* **182**, 5693–5701 (2009).
77. A. Huang *et al*., Increased CD14(+)HLA-DR (-/low) myeloid-derived suppressor cells correlate with extrathoracic metastasis and poor response to chemotherapy in non-small cell lung cancer patients. *Cancer Immunol. Immunother.* **62**, 1439–1451 (2013).
78. B. Huang *et al*., Gr-1+CD115+ immature myeloid suppressor cells mediate the development of tumor-induced T regulatory cells and T-cell anergy in tumor-bearing host. *Cancer Res.* **66**, 1123–1131 (2006).
79. W. Peng *et al*., PD-1 blockade enhances T-cell migration to tumors by elevating IFN-γ inducible chemokines. *Cancer Res.* **72**, 5209–5218 (2012).
80. H. Dong *et al*., Tumor-associated B7-H1 promotes T-cell apoptosis: A potential mechanism of immune evasion. *Nat. Med.* **8**, 793–800 (2002).
81. K. Sakuishi *et al*., Targeting Tim-3 and PD-1 pathways to reverse T cell exhaustion and restore anti-tumor immunity. *J. Exp. Med.* **207**, 2187–2194 (2010).
82. K. Woroniecka *et al*., T-cell exhaustion signatures vary with tumor type and are severe in glioblastoma. *Clin. Cancer Res.* **24**, 4175–4186 (2018).